DELPHI Collaboration DELPHI 2005-006 CONF 726
31 May 2005

Study of Trilinear Gauge Boson Couplings ZZZ, $ZZ\gamma$ and $Z\gamma\gamma$ at LEP

E. Graziani
INFN - Roma Tre
C. Matteuzzi
Università di Milano and INFN
L. Pieri
Università di Roma Tre, and INFN[1]
R.L. Sekulin
Rutherford Appleton Laboratory
V. Verzi
Università di Roma II and INFN
O. Yushchenko
IHEP, Serpukov

Abstract

Trilinear neutral gauge boson couplings ZZZ, $ZZ\gamma$ and $Z\gamma\gamma$ have been studied with the DELPHI detector using data at energies between 183 and 208 GeV. Limits are derived on these couplings from an analysis of the reactions $e^+e^-\to Z\gamma$, using data from the final states $\gamma f\bar{f}$, with $f = q$ or ν, from $e^+e^-\to ZZ$, using data from the four-fermion final states $q\bar{q}q\bar{q}$, $q\bar{q}\mu^+\mu^-$, $q\bar{q}e^+e^-$, $q\bar{q}\nu\bar{\nu}$, $\mu^+\mu^-\nu\bar{\nu}$ and $e^+e^-\nu\bar{\nu}$, and from $e^+e^-\to Z\gamma^*$, in which the final state γ is off mass-shell, using data from the four-fermion final states $q\bar{q}e^+e^-$ and $q\bar{q}\mu^+\mu^-$. No evidence for the presence of such couplings is observed, in agreement with the predictions of the Standard Model.

Contributed Paper for LP 2005 (Uppsala) and HEP-EPS 2005 (Lisbon)

[1]Now at Stockholm University

1 Introduction

One of the important predictions of the Standard Model which can be tested at LEP2 is its non-Abelian character, leading to the prediction of triple-gauge-boson couplings. However, while non-zero values of these couplings are predicted for the charged ($WW\gamma$, WWZ) sector, the $SU(2) \times U(1)$ symmetry of the Standard Model predicts the absence of such couplings in the neutral sector, namely at the ZZZ, $ZZ\gamma$ and $Z\gamma\gamma$ vertices. This paper describes an investigation of this prediction by DELPHI using LEP2 data taken between 1997 and 2000 at energies between 183 and 208 GeV.

1.1 Phenomenology of the neutral triple-gauge-boson vertex

Within the Standard Model, production of two neutral gauge bosons in e^+e^- collisions proceeds at lowest order via the t- or u-channel exchange of an electron. These processes are shown in figures 1a) and b), where both on- and off-shell γ production is implied, as is the subsequent decay of the final state Z or off-shell γ into a fermion-antifermion pair. Figure 1c) shows a contribution to production of the same final states which could come from physics beyond the Standard Model by the s-channel exchange of a virtual γ or Z via a neutral triple-gauge-boson coupling. In the reactions $e^+e^- \rightarrow Z\gamma$ and $e^+e^- \rightarrow ZZ$ the final state can, to a good approximation, be considered to be of two on-shell bosons, so that only the exchanged boson at the triple-gauge-boson vertex need necessarily be considered as off-shell, while in the reaction $e^+e^- \rightarrow Z\gamma^*$ both the exchanged boson and the outgoing γ^* are off-shell. A further process containing a neutral triple-gauge-boson coupling with two of the bosons off-shell is shown in figure 1d); here a single Z is produced in the final state Ze^+e^- via fusion of two exchanged vector bosons.

The phenomenology of the case where two of the three neutral gauge bosons interacting at the $V_1^0V_2^0V_3^0$ vertex are on mass-shell has been described in [1]. In this case, there are twelve independent anomalous couplings satisfying Lorentz invariance and Bose symmetry. Calling V the exchanged boson ($V = Z, \gamma$), the couplings f_i^V (i =4,5) produce a ZZ final state and h_i^V ($i = 1 \cdots 4$) the $Z\gamma$ final state. The couplings f_5^V, h_3^V and h_4^V are CP-conserving and f_4^V, h_1^V and h_2^V are CP-violating. There are no couplings common to production of both the ZZ and $Z\gamma$ final states.

A complete phenomenological description of the anomalous neutral gauge couplings in the case where one, two or three of the gauge bosons interacting at the $V_1^0V_2^0V_3^0$ vertex may be off mass-shell has been developed in [2]. Following the treatment of the charged triple-gauge-boson vertex developed, for instance, in [3, 4], all the Lorentz invariant forms which can contribute to the ZZZ, $ZZ\gamma$ and $Z\gamma\gamma$ vertices are listed, imposing Bose symmetry as appropriate. An effective Lagrangian model is then developed in terms of the operators of lowest dimension which are required to reconstruct fully all the vertex forms, and which affect only the neutral triple-gauge-boson vertex.[2] This leads to a Lagrangian with operators of dimension, d, ranging from $d = 6$ to $d = 12$. Such an expansion is valid in the case where the new physics energy scale, Λ, represented by the operators is very high, *i.e.* $\Lambda \gg m_Z$, and the relative contribution from an operator of dimension d may be expected

[2]The $V_1^0V_2^0V_3^0$ vertex functions receive contributions from both transverse and scalar terms, the latter contributing in the case where one off-shell Z decays to a heavy fermion pair through its axial coupling. In the analysis of LEP data only transverse terms need be considered, due to the negligible contribution of $Z \rightarrow t\bar{t}$ decays. The contribution of scalar terms is therefore ignored in the following.

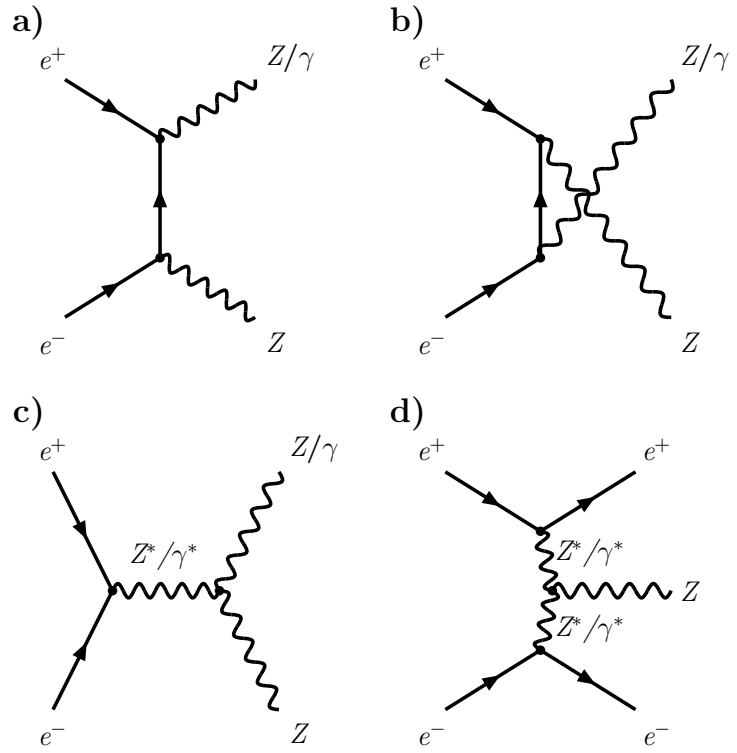

Figure 1: a), b) Lowest order Feynman diagrams for the production of two gauge bosons ZZ and $Z\gamma$ by Standard Model processes, where both on- and off-shell γ production is implied. c) Production of the same final states via an anomalous interaction among three neutral gauge bosons. d) Production of the Ze^+e^- final state via an anomalous neutral triple-gauge-boson coupling.

to be suppressed by a factor $1/\Lambda^{(d-4)}$. In the analysis we report here, we have considered only the lowest dimension operators contributing to the parameters we have determined. In addition to satisfying Lorentz and Bose symmetry, the operators are required to be $U(1)_{em}$-invariant, and both CP-conserving operators, $\mathcal{O}$, and CP-violating operators, $\tilde{\mathcal{O}}$, with coefficients ℓ and $\tilde{\ell}$, respectively, are considered:

$$\mathcal{L} = e\Big(\sum_{i,CP+} \ell_i^{V_1^0V_2^0V_3^0}\mathcal{O}_i^{V_1^0V_2^0V_3^0} + \sum_{i,CP-} \tilde{\ell}_i^{V_1^0V_2^0V_3^0}\tilde{\mathcal{O}}_i^{V_1^0V_2^0V_3^0}\Big)\,. \tag{1}$$

Of the operators included in the sum defined above, some affect the V^0ZZ and $V^0Z\gamma^*$ vertices ($V^0 \equiv Z, \gamma$), some the $V^0Z\gamma^*$ vertex only, and some the $V^0Z\gamma^*$ and $V^0Z\gamma$ vertices; none contribute to all three vertices. In [2] a connection is made between the coefficients ℓ_i and $\tilde{\ell}_i$ of the operators in the effective Lagrangian describing the general $V_1^0V_2^0V_3^0$ vertex and the dimensionless coefficients h and f describing on-shell $Z\gamma$ and ZZ production, respectively: retaining only the terms corresponding to contributions from operators of lowest dimension, each of the coefficients h_1^V, h_3^V, f_4^V and f_5^V (which are dimensionless) is related to one operator of dimension $d = 6$ by $f, h = \ell^{V_1^0V_2^0V_3^0} m_Z^2$. The lowest dimension operators contributing to h_2^V and h_4^V have $d = 8$.

As in the case of the charged triple-gauge-boson couplings, a further simplification in the possible structure of the effective Lagrangian is obtained by imposition of $SU(2)\times U(1)$ invariance on its form. Such a form is presented in an addendum to [2], and the effective

Lagrangian reduces to a sum of two terms, both with dimension $d = 8$, one ($\mathcal{O}_{SU(2)\times U(1)}$) CP-conserving and one ($\tilde{\mathcal{O}}_{SU(2)\times U(1)}$) CP-violating. This simplification leads to constraints between some of the ${\ell_i}^{V_1^0 V_2^0 V_3^0}$ or ${\tilde{\ell}_i}^{V_1^0 V_2^0 V_3^0}$ defined in equation (1):

$$ {\ell_1}^{ZZZ} \cot\theta_W = {\ell_1}^{ZZ\gamma} = -{\ell_2}^{ZZ\gamma} = -{\ell_1}^{Z\gamma\gamma} \tan\theta_W = \frac{v^2}{4}\ell_{SU(2)\times U(1)} \ , \tag{2} $$

$$ {\tilde{\ell}_1}^{ZZZ} \cot\theta_W = {\tilde{\ell}_1}^{ZZ\gamma} = -{\tilde{\ell}_3}^{ZZ\gamma} = -{\tilde{\ell}_1}^{Z\gamma\gamma} \tan\theta_W = \frac{v^2}{4}\tilde{\ell}_{SU(2)\times U(1)} \ , \tag{3} $$

where θ_W is the weak mixing angle, v is the vacuum expectation value of the Higgs field and $\ell_{SU(2)\times U(1)}$, $\tilde{\ell}_{SU(2)\times U(1)}$ are the coefficients of the operators $\mathcal{O}_{SU(2)\times U(1)}$ and $\tilde{\mathcal{O}}_{SU(2)\times U(1)}$, respectively. If applied solely to the on-shell channels $Z\gamma$ and ZZ, these conditions become, respectively:

$$ f_5^Z \cot\theta_W = h_3^Z = -f_5^\gamma = h_3^\gamma \tan\theta_W = m_Z^2 \frac{v^2}{4}\ell_{SU(2)\times U(1)} \ , \tag{4} $$

$$ f_4^Z \cot\theta_W = h_1^Z = -f_4^\gamma = h_1^\gamma \tan\theta_W = m_Z^2 \frac{v^2}{4}\tilde{\ell}_{SU(2)\times U(1)} \ . \tag{5} $$

The $SU(2) \times U(1)$-conserving Lagrangian considered in [2] is constructed so as to affect only the neutral gauge boson and Higgs sectors, and an alternative form, which would additionally affect off-mass-shell charged gauge boson production, has been proposed in [5]. This leads to a Lagrangian with four possible terms, two CP-conserving ($\mathcal{O}_8^A$, $\mathcal{O}_8^B$) and two CP-violating ($\tilde{\mathcal{O}}_8^A$, $\tilde{\mathcal{O}}_8^B$) and hence to looser constraints between the possible contributing operators: in each of the sets of conditions (2) - (5) listed above, the relations corresponding in the diagrams of figure 1 to γ and Z exchange decouple, giving, for instance in the case of (2), the separate conditions

$$ {\ell_1}^{ZZZ} \cot\theta_W = {\ell_1}^{ZZ\gamma} \text{ and } {\ell_2}^{ZZ\gamma} = {\ell_1}^{Z\gamma\gamma} \tan\theta_W \ , \tag{6} $$

with an analogous separation in conditions (3) - (5). This leads to four coefficients, $\ell_8^{A,B}$, $\tilde{\ell}_8^{A,B}$, related to the respective Lagrangian operators by appropriate factors of m_Z and v. In both the stronger and weaker of these sets of constraints (which we refer to as the Gounaris-Layssac-Renard and Alcaraz constraints, with respect to the authorship of references [2] and [5]), the gauge invariant operators all now contribute to all three neutral trilinear gauge boson vertices, V^0ZZ, $V^0Z\gamma^*$ and $V^0Z\gamma$.

In order to study the $V_1^0V_2^0V_3^0$ vertex, three physical final states have been defined from the data: $Z\gamma$, $Z\gamma^*$ and ZZ. The first of these is a three-body final state comprising the Z decay products and a detected photon, while the other two are four-fermion final states with, respectively, one or two fermion-antifermion pairs having mass in the Z region. Given the phenomenology summarized above, we have then chosen to determine the following parameters in our study:

- Using data from the final states ZZ and $Z\gamma^*$, values are determined for the coefficients of each of the four $d = 6$ operators which are related in the on-shell limit to one of the f coefficients defined in the on-shell formalism of reference [1]. Similarly, using data from the final states $Z\gamma$, $Z\gamma^*$ and ZZ, values of the coefficients of the four $d = 6$ operators related to the on-shell h coefficients are determined. In the latter case, the ZZ data are used as well as the $Z\gamma^*$, as the off-shell γ couples to the $f\bar{f}$

system over the whole of the four-fermion phase space. However, in these studies the statistical contribution of the off-shell final states compared to that of on-shell $Z\gamma$ or ZZ production is very small, so that the values of the parameters determined, quoted in dimensionless form, $\ell^{V_1^0 V_2^0 V_3^0} m_Z^2$, are directly comparable with published results using data from on-shell channels, and the relevant respective likelihood distributions may be combined.

- The $V^0 Z\gamma^*$ vertex is studied on its own by determining the coefficients of the lowest dimension operators which affect solely these vertices. There are two such operators, both of dimension $d = 8$, one CP-conserving and involving s-channel γ exchange in the production process, and the other CP-violating and involving s-channel Z exchange. Again, data from both the $Z\gamma^*$ and ZZ final states were used in the determination of the coefficients of these operators, and the coefficients are quoted in dimensionless form: $\ell^{V_1^0 V_2^0 V_3^0} m_Z^4$.

- The coefficients of the $SU(2) \times U(1)$-conserving operators are determined, using both the Gounaris-Layssac-Renard and the Alcaraz constraints. They are quoted in a dimensionless form, such that in the on-shell limit they become equal to one of the h_i^V occurring in the constraint equations (4) and (5) above.

A list of the parameters we have determined, the definitions of the operators to which they refer and (where relevant) the on-shell coefficients to which they are related is given in table 1.

1.2 Experimental considerations

Of the three final state channels, $Z\gamma$, ZZ and $Z\gamma^*$, defined in the previous section, the most precise limits on anomalous couplings are derived from the first, when the final state photon is on-shell. In this channel, the kinematic region with high photon energy and large photon polar angle is most sensitive to the anomalous couplings, and in this region the anomalous interactions give rise to a change in the total rate and to an enhancement of the production of longitudinally polarized Z bosons. Our analysis covers two reactions to which the diagrams describing $Z\gamma$ production provide the dominant contribution: $e^+e^- \to \nu\overline{\nu}\gamma$, in which the observed number of events is compared with the number predicted from the total cross-section for this process, and $e^+e^- \to q\bar{q}\gamma$, with the $q\bar{q}$ system coming predominantly from Z decay, in which the distribution of the decay angle of the Z in its rest frame with respect to the direction of the Z in the overall centre of mass is studied. The present analysis uses data from LEP2 at energies ranging from 189 to 208 GeV. Previous DELPHI results on this channel can be found in [6]; they used data with energies up to $\sqrt{s} = 172$ GeV, and the limits were obtained using an analysis based only on the value of the observed total cross-section.

The total ZZ cross-section is also sensitive to the anomalous couplings, and the sensitivity increases strongly with $\sqrt{s}$. Large interference between Standard Model and anomalous amplitudes arises for CP-conserving couplings (especially for f_5^Z) when considering the differential cross-section $d\sigma/d|\cos\theta_Z|$, where θ_Z is the Z production angle with respect to the beam axis. The analysis reported here is based on a study of this differential distribution in the LEP2 data in the energy range 183 to 208 GeV. DELPHI has previously reported a study of the ZZ production cross-section in all visible $f_1\bar{f}_2 f_3 \bar{f}_4$

Vertices affected	Parameter	Lagrangian Operator	Related on-shell coefficient
a)			
ZZZ	$\tilde{\ell}_1^{ZZZ} m_Z^2$	$-Z_\sigma(\partial^\sigma Z_\nu)(\partial_\mu Z^{\mu\nu})$	f_4^Z
	$\ell_1^{ZZZ} m_Z^2$	$\tilde{Z}_{\mu\nu}(\partial_\sigma Z^{\sigma\mu})Z^\nu$	f_5^Z
$ZZ\gamma$	$\tilde{\ell}_3^{ZZ\gamma} m_Z^2$	$-(\partial_\mu F^{\mu\beta})Z_\alpha(\partial^\alpha Z_\beta)$	f_4^γ
	$\ell_2^{ZZ\gamma} m_Z^2$	$\tilde{Z}^{\mu\nu} Z_\nu(\partial^\sigma F_{\sigma\mu})$	f_5^γ
	$\tilde{\ell}_1^{ZZ\gamma} m_Z^2$	$-F^{\mu\beta} Z_\beta(\partial^\sigma Z_{\sigma\mu})$	h_1^Z
	$\ell_1^{ZZ\gamma} m_Z^2$	$-\tilde{F}_{\mu\nu} Z^\nu(\partial_\sigma Z^{\sigma\mu})$	h_3^Z
$Z\gamma\gamma$	$\tilde{\ell}_1^{Z\gamma\gamma} m_Z^2$	$-(\partial^\sigma F_{\sigma\mu})Z_\beta F^{\mu\beta}$	h_1^γ
	$\ell_1^{Z\gamma\gamma} m_Z^2$	$-\tilde{F}_{\rho\alpha}(\partial_\sigma F^{\sigma\rho})Z^\alpha$	h_3^γ
b)			
$ZZ\gamma$	$\tilde{\ell}_4^{ZZ\gamma} m_Z^4$	$\partial^\mu F_{\mu\nu}(\Box\partial^\nu Z_\alpha)Z^\alpha$	–
$Z\gamma\gamma$	$\ell_2^{Z\gamma\gamma} m_Z^4$	$\Box\tilde{F}^{\mu\nu}(\partial^\sigma F_{\sigma\mu})Z_\nu$	–
c) i)			
ZZZ $ZZ\gamma$ $Z\gamma\gamma$	$-\cot\theta_W m_Z^2 \frac{v^2}{4}\tilde{\ell}_{SU(2)\times U(1)}$	$iB_{\mu\nu}(\partial_\sigma B^{\sigma\mu})(\Phi^\dagger D^\nu\Phi)$	h_1^γ
	$-\cot\theta_W m_Z^2 \frac{v^2}{4}\ell_{SU(2)\times U(1)}$	$i\tilde{B}_{\mu\nu}(\partial_\sigma B^{\sigma\mu})(\Phi^\dagger D^\nu\Phi)$	h_3^γ
ii)			
$ZZ\gamma$	$-\cot\theta_W m_Z^2 \frac{v^2}{4}\tilde{\ell}_8^A$	$iB_{\mu\nu}(\partial_\sigma B^{\sigma\mu})(\Phi^\dagger D^\nu\Phi)$	h_1^γ
	$-\cot\theta_W m_Z^2 \frac{v^2}{4}\ell_8^A$	$i\tilde{B}_{\mu\nu}(\partial_\sigma B^{\sigma\mu})(\Phi^\dagger D^\nu\Phi)$	h_3^γ
ZZZ $Z\gamma\gamma$	$-\cot\theta_W m_Z^2 \frac{v^2}{4}\tilde{\ell}_8^B$	$iB_{\mu\nu}(\partial_\sigma W_I^{\sigma\mu})(\Phi^\dagger\tau_I D^\nu\Phi)$	h_1^Z
	$-\cot\theta_W m_Z^2 \frac{v^2}{4}\ell_8^B$	$i\tilde{B}_{\mu\nu}(\partial_\sigma W_I^{\sigma\mu})(\Phi^\dagger\tau_I D^\nu\Phi)$	h_3^Z

Table 1: Parameters determined in this study, corresponding Lagrangian operators in the models of references [2] and [5], and (where appropriate) related on-shell parameters: a) Coefficients of lowest dimension operators contributing to ZZ and $Z\gamma^*$ production or to $Z\gamma^*$ and $Z\gamma$ production; b) Coefficients of lowest dimension operators affecting only the $V^0 Z\gamma^*$ vertices; c) Coefficients of $SU(2)\times U(1)$-conserving operators according to i) the Gounaris-Layssac-Renard constraints and ii) the Alcaraz constraints. The constraints are given in the text. The vertices $V_1^0 V_2^0 V_3^0$ affected by these operators (without distinguishing the V_i^0 as on- or off-mass-shell) are indicated in column 1. The fields Z_μ, F_μ, B_μ and W_μ represent the Z, photon, $U(1)_Y$ and $SU(2)_L$ fields, respectively; $\tilde{Z}_{\mu\nu}$, $\tilde{F}_{\mu\nu}$ and $\tilde{B}_{\mu\nu}$ are the contractions of the respective field tensors with the four-dimensional antisymmetric tensor; Φ is the Higgs field and v its vacuum expectation value, D represents the covariant derivative of $SU(2)\times U(1)$, and τ_I are the Pauli matrices.

final states in these data [7]. The same sets of identified events have been used in the present analysis, with the exception of the $q\bar{q}\tau^+\tau^-$, $\tau^+\tau^-\nu\bar{\nu}$ and $l^+l^-l^+l^-$ channels, which are not used.

In a separate publication [8], DELPHI has studied the $Z\gamma^*$ final state in the same LEP2 data as used for the channels described above, reporting on a comparison of the cross-section for $Z\gamma^*$ production in various channels with Standard Model predictions. We use the samples identified in [8] in the $q\bar{q}e^+e^-$ and $q\bar{q}\mu^+\mu^-$ final states in the present analysis, which thus represents an interpretation of these data for the first time in terms of possible anomalous gauge couplings. The data were examined as a function of the bidimensional ($M_{l^+l^-}$, $M_{q\bar{q}}$) mass distribution, requiring one of them to be in the region of the Z mass, and they were also divided into two regions of the l^+l^- polar angle with respect to the beam direction (equivalent to the variable θ_Z used in the analysis of ZZ events).

Limits on anomalous neutral gauge couplings in the $Z\gamma$ and ZZ final states have been reported by other LEP experiments; recent published results may be found in the papers listed in [9].

2 Experimental details and analysis

Events were recorded in the DELPHI detector. Detailed descriptions of the DELPHI components can be found in [10] and the description of its performance, as well as of the trigger system [11] and of the luminosity monitor, can be found in [12]. For LEP2 operations, the vertex detector was upgraded [13], and a set of scintillation counters was added to veto photons in the blind regions of the electromagnetic calorimetry at polar angles around $\theta = 40^\circ$. The performance of the detector was simulated using the program DELSIM [12], which was interfaced to the programs used in the generation of Monte Carlo events and to the programs used to simulate the hadronization of quarks from Z and γ^* decay or from background processes. During the year 2000, one sector (1/12) of the time projection chamber, DELPHI's main tracking device, was inactive for about a quarter of the data-taking period. The effect of this was taken into account in the detector simulation and in the determination of cross-sections from the data.

The selection of events in the three physical final states, $Z\gamma$, ZZ and $Z\gamma^*$, considered in this paper, and the simulation of the processes contributing to signals and backgrounds are described in the following subsections. In the case of the ZZ and $Z\gamma^*$ samples, the reader is referred to recent DELPHI publications on the production of these final states (references [7, 8], respectively) for a full description of the event selection procedures. The event samples used in the present analysis of these two final states have been selected using essentially identical procedures to those described in [7, 8], and cover the same energy range (183 - 208 GeV). These procedures are summarized, respectively, in sections 2.2 and 2.3 below, and any changes from the methods described in [7, 8] are mentioned. DELPHI has also reported a study of events observed at LEP2 in which only photons and missing energy were detected [14]. The present analysis uses data in the part of the kinematic region covered in [14] in which a high energy photon is produced at a large angle with respect to the beam direction; data in the energy range 189 - 208 GeV have been used. The selection procedures specific to this final state as well as to that in which a quark-antiquark pair is produced, rather than missing energy, are described in section 2.1

below.

In the final year of LEP running, data were taken over a range of energies from 205 to 208 GeV. The values of the centre-of-mass energy quoted in the descriptions below for that year correspond to the averages for the data samples collected.

2.1 The $Z\gamma$ final state

The selection procedure for $Z\gamma$ production in the kinematic region with greatest sensitivity to anomalous gauge couplings concentrated on a search for events with a very energetic photon in the angular range $45^\circ < \theta_\gamma < 135^\circ$, where θ_γ is the polar angle of the photon with respect to the beam direction. This angular region is covered by DELPHI's barrel electromagnetic calorimeter, the High density Projection Chamber (HPC). The search was conducted in events with two final state topologies: $\nu\overline{\nu}\gamma$ and $q\bar{q}\gamma$.

The $\nu\overline{\nu}\gamma$ sample was selected from events with a detected final state containing only a single photon. Its energy, E_γ, was required to be greater than 50 GeV and only photons in the range covered by the HPC, $45^\circ < \theta_\gamma < 135^\circ$ were accepted. No tracks or hits were allowed in DELPHI's main tracking detector, the time projection chamber. It was also required that no electromagnetic showers with energy exceeding defined background noise levels were present in the forward electromagnetic calorimeter and the luminosity monitor. Further showers in the HPC were accepted only if they were within 20° of the first one, and such showers were then combined. Cosmic ray events were suppressed by requiring that any signal in the hadronic calorimeter be in the same angular region as the signal in the electromagnetic calorimeter, and that the electromagnetic shower point towards the beam collision point within an angle of 15°. The trigger efficiency was measured using Compton and Bhabha events. The expected numbers of events were calculated using the generators NUNUGPV, based on [15], and KORALZ [16], interfaced to the full DELPHI simulation program. From these simulations, the efficiency for detecting $\nu\overline{\nu}\gamma$ events in the kinematic region considered here was estimated to be in the region of 50%, independent of the centre-of-mass energy. Contributions from background sources to this channel were estimated to be negligible. The results obtained applying these criteria are shown in table 2. Full details of the analysis of this final state may be found in [14]. The distribution of the energy of identified photons normalized to the beam energy, E_γ/E_{beam}, in the data collected in the $\nu\overline{\nu}\gamma$ channel before imposing the cut at $E_\gamma = 50$ GeV is shown in figure 2a), which also shows the expectation of the Standard Model.

In the selection of events in the $q\bar{q}\gamma$ channel, the same requirements were imposed on the energy and polar angle of photon candidates as in the $\nu\overline{\nu}\gamma$ case, namely: $E_\gamma > 50$ GeV and $45^\circ < \theta_\gamma < 135^\circ$. In addition, events were required to have six or more charged particle tracks, each with length greater than 20 cm, momentum greater than 200 MeV/c, polar angle between 10° and 170°, and transverse and longitudinal impact parameters at the interaction point of less than 4 cm. The total charged energy in the event was required to exceed $0.10\sqrt{s}$ and the effective energy of the collision [17], excluding the detected photon, $\sqrt{s'}$, was required to satisfy $\sqrt{s'} < 130$ GeV. Jets were reconstructed using the LUCLUS [18] algorithm and, omitting the γ, the event was forced into a two-jet configuration. The identified photon was required to be isolated from the nearest jet axis by at least 20°. The efficiency, purity and the expected numbers of events from other processes were computed using events generated with PYTHIA [18], relying on JETSET 7.4 [18] for quark fragmentation, and interfaced to the full DELPHI simulation program.

$\sqrt{s}$ (GeV)	Integrated luminosity (pb^{-1})	Selected data	Total predicted events
188.6	154.7	87	89.2
191.6	25.1	14	13.1
195.5	76.2	32	37.5
199.5	83.1	45	38.5
201.6	40.6	20	18.2
206.1	214.6	98	102.3
Total	594.3	296	298.8

Table 2: $\nu\overline{\nu}\gamma$ final state: Integrated luminosity and numbers of observed and expected events at each energy, $\sqrt{s}$.

The main background processes, contributing about 3% of the sample, came from $q\bar{q}$ production with a photon from fragmentation of one of the quarks or from initial state radiation, and from WW production. From these simulations, the efficiency for detecting $q\bar{q}\gamma$ events in the kinematic region considered here was estimated to be in the region of 77%, independent of the centre-of-mass energy. The results obtained applying this procedure are shown in table 3.

$\sqrt{s}$ (GeV)	Integrated luminosity (pb^{-1})	Selected data	Total predicted events	Expected background
188.6	154.3	454	467.3	14.9
191.6	25.4	79	75.0	2.6
195.5	77.1	203	214.1	5.8
199.5	84.2	208	225.5	5.9
201.6	40.6	130	104.5	2.8
205.9	218.8	507	515.1	13.9
Total	600.4	1581	1601.5	45.9

Table 3: $q\bar{q}\gamma$ final state: Integrated luminosity, numbers of observed and expected events, and predicted background contribution at each energy, $\sqrt{s}$.

Summing over all energy points, totals of 296 and 1581 events were observed in the $\nu\overline{\nu}\gamma$ and $q\bar{q}\gamma$ channels, respectively. These numbers may be compared with the totals expected from simulated production of these final states by Standard Model processes: 298.8 events in $\nu\overline{\nu}\gamma$, and 1601.5 events in $q\bar{q}\gamma$.

In the $\nu\overline{\nu}\gamma$ channel, values of the gauge boson coupling parameters were derived by comparing the observed number of events with that predicted from the total cross-section for this process, while in the $q\bar{q}\gamma$ channel a fit was performed to the distribution of the decay angle, $\alpha^\star$, of the Z in its rest frame with respect to the direction of the Z in the overall centre of mass. The value of $\alpha^\star$ was estimated from the directions of the vectors in the laboratory frame $\mathbf{p}_\gamma$ and $\mathbf{p_i}$ of the reconstructed photon and jets ($i = 1, 2$), respectively, as:

$$\cot\alpha^\star = \gamma\left(\cot\alpha_1 - \frac{\beta}{\sin\alpha_1}\right), \tag{7}$$

$$\text{with}\ \ \beta = \frac{\sin(\alpha_1+\alpha_2)}{\sin\alpha_1+\sin\alpha_2},\ \ \cos\alpha_{\rm i} = -\frac{\mathbf{p}_\gamma\cdot\mathbf{p}_{\rm i}}{|\mathbf{p}_\gamma|\cdot|\mathbf{p}_{\rm i}|}\ \ \text{and}\ \ \gamma = \frac{1}{\sqrt{1-\beta^2}}\ . \tag{8}$$

The distribution of $\cos\alpha^\star$ for the data selected in the $q\bar{q}\gamma$ channel is shown in figure 2b) and compared with the predictions of the Standard Model and of a non-standard scenario with $h_3^\gamma = \pm 0.2$. The predictions for non-zero neutral gauge boson couplings were made by reweighting the simulated samples produced according to the Standard Model with the calculations of Baur and Berger [19][3].

2.2 The ZZ final state

The study of the triple-gauge-boson vertex in ZZ production used the samples of events selected in the $q\overline{q}q\overline{q}$, $q\bar{q}\mu^+\mu^-$, $q\bar{q}e^+e^-$, $q\bar{q}\nu\bar{\nu}$, $\mu^+\mu^-\nu\bar{\nu}$ and $e^+e^-\nu\bar{\nu}$ final states. The procedures used to extract the data have been described fully in [7]; we give here a brief summary of the methods used in the selection of events in each of these final states, and provide a table of the total numbers of events observed and expected for production of each of them by Standard Model processes.

The $ZZ \to q\overline{q}q\overline{q}$ process represents 49% of the ZZ decay topologies and produces four or more jets in the final state. After a four-jet preselection, the ZZ signal was identified within the large background from WW and $q\bar{q}\gamma$ production by evaluating a probability that each event came from ZZ production, based on invariant-mass information, on the b-tag probability per jet and on topological information.

The process $e^+e^- \to q\bar{q}l^+l^-$ has a branching ratio in ZZ production of 4.7% per lepton flavour. High efficiency and high purity were attained with a cut-based analysis using the clear experimental signature provided by the two leptons, which are typically well isolated from all other particles. The on-shell ZZ sample was selected by applying simultaneous cuts on the masses of the l^+l^- pair, on the remaining hadronic system and on their sum.

The decay mode $q\bar{q}\nu\bar{\nu}$ represents 28% of the ZZ final states. The signature of this decay mode is a pair of jets, acoplanar with respect to the beam axis, with visible and recoil masses compatible with the Z mass. The most difficult backgrounds arise from single resonant $We\nu_e$ production, from WW production where one of the W bosons decays into $\tau\nu_\tau$, and from $q\bar{q}$ events accompanied by energetic isolated photons escaping detection. The selection of events was made using a combined discriminant variable obtained with an Iterative Discriminant Analysis program (IDA) [21].

The final state $l^+l^-\nu\bar{\nu}$ has a branching ratio in ZZ production of 1.3% per charged lepton flavour. Events with $l \equiv \mu, e$ were selected with a sequential cut-based analysis. The on-shell ZZ sample was selected from the events assigned to this final state by applying cuts on the masses of the l^+l^- pair and of the system recoiling against it. The most significant background in the sample is from WW production with both Ws decaying leptonically.

In the estimation of the expected numbers of events in all the final states discussed above, processes leading to a four-fermion final state were simulated with EXCALIBUR [22], with JETSET 7.4 used for quark fragmentation. Amongst the background

[3]The code used was modified by a factor i according to the correction suggested by Gounaris *et al* [20].

processes leading to the final-state toplogies described above, GRC4F [23] was used to simulate $We\nu$ production, PYTHIA for $q\bar{q}(\gamma)$, KORALZ for $\mu^+\mu^-(\gamma)$ and $\tau^+\tau^-(\gamma)$, BHWIDE [24] for $e^+e^-(\gamma)$, and TWOGAM [25] and BDK [26] for two-photon processes.

The presence of anomalous neutral trilinear gauge boson couplings in the data samples described above was investigated by studying the distribution of the Z production polar angle, $|\cos\theta_Z|$. For events in the $q\bar{q}\nu\bar{\nu}$ and $l^+l^-\nu\bar{\nu}$ final states, the Z direction was taken to be the direction of the reconstructed di-jet or l^+l^- pair, respectively, while in the $q\bar{q}l^+l^-$ final state, the Z direction was evaluated following a 4-constraint kinematic fit to the jet and lepton momenta, imposing four-momentum conservation. In the $q\overline{q}q\overline{q}$ final state, the indistinguishability of the jets leads to three possible jet-jet pairs, each of which could come from ZZ decay. A 5-constraint kinematic fit was performed on each of these combinations, imposing four-momentum conservation and equality of the masses of the two jet pairs. The fit with the minimum value of χ^2 was retained and the value of $|\cos\theta_Z|$ evaluated from the fitted jet directions.

Figure 3 shows the distribution of $|\cos\theta_Z|$ for a high purity sample of ZZ data, composed of the $q\bar{q}l^+l^-$ and $l^+l^-\nu\bar{\nu}$ samples defined above and, for illustrative purposes, samples of $q\overline{q}q\overline{q}$ and $q\bar{q}\nu\bar{\nu}$ events defined by stringent cuts on the probabilistic variables used in these channels ($q\overline{q}q\overline{q}$ probability > 0.55, and $q\bar{q}\nu\bar{\nu}$ IDA variable > 3), so as to suppress the background levels present. (As described below, no cuts were imposed on these variables in the determination of coupling parameters). The figure also shows the Standard Model expectations and the distributions predicted for values of $f_5^Z = \pm 1.5$. The content of this sample is shown in table 4. The values quoted in the table for signal selection efficiencies are defined as the fraction of events of the relevant four-fermion final state present in the selected sample, while the estimated backgrounds refer to contributions from other channels.

Channel	Integrated luminosity (pb^{-1})	Selected data	Total predicted events	Expected background	Selection efficiency
$q\overline{q}q\overline{q}$	665.1	76	69.4	22.1	0.18
$q\bar{q}\mu^+\mu^-$	665.3	21	22.0	1.1	0.86
$q\bar{q}e^+e^-$	665.3	19	23.7	2.6	0.73
$q\bar{q}\nu\bar{\nu}$	639.0	45	55.5	22.3	0.21
$l^+l^-\nu\bar{\nu}$	665.3	10	8.9	4.7	0.30
Total	–	171	179.5	52.8	–

Table 4: ZZ production: Integrated luminosity, numbers of observed and expected events, predicted background contribution and estimated selection efficiency for each topological final state, summed over all energies.

In the determination of the coupling parameters, extended maximum-likelihood fits were made to the distribution of $|\cos\theta_Z|$ for data from the channels selected with cut-based analyses ($q\bar{q}l^+l^-$ and $l^+l^-\nu\bar{\nu}$), while for the channels selected using probabilistic methods ($q\overline{q}q\overline{q}$ and $q\bar{q}\nu\bar{\nu}$), a simultaneous fit was made to the distributions of $|\cos\theta_Z|$ and of the discriminant variable (the ZZ probability for $q\overline{q}q\overline{q}$ and the IDA output variable for $q\bar{q}\nu\bar{\nu}$), without applying any cuts on the values of these variables.

The predictions for non-zero neutral gauge boson couplings were made by reweighting the simulated samples produced according to the Standard Model with the calculations of the DELTGC [27] event generator, which adds the amplitude from hypothesized neutral trilinear gauge boson vertices to all the other amplitudes contributing to the production of any four-fermion final state.

2.3 The $Z\gamma$* final state

In a separate publication [8], DELPHI has reported on a study of $Z\gamma^*$ production in LEP2 data, and in particular on a comparison of the observed cross-section with Standard Model predictions, using data from a variety of four-fermion final state topologies involving both hadronic and leptonic Z decay modes. In the present analysis, we interpret data in the $q\bar{q}\mu^+\mu^-$ and $q\bar{q}e^+e^-$ final states in terms of possible anomalous trilinear gauge boson interactions. These two channels are chosen because the two final state leptons are typically well isolated from all other particles, allowing such events to be selected with high efficiency over the whole region of γ^* mass. Events with either the l^+l^- or the $q\bar{q}$ invariant mass in the vicinity of the Z mass and the other invariant mass not in the Z region were then used in the estimation of possible anomalous gauge coupling parameters. Full details of the selection procedure are given in [8]; a summary of the main features follows.

Events containing total charged hadronic energy above $0.3\sqrt{s}$ and at least two lepton candidates of the same flavour and opposite charge were selected. All particles except the lepton candidates were clustered into jets and a kinematic fit requiring four-momentum conservation was applied. At least one of the two lepton candidates was required to satisfy strong lepton identification criteria, while softer requirements were specified for the second. In order to increase the purity of the selection, further cuts were made in two discriminating variables: P_t^{min}, the lesser of the transverse momenta of the lepton candidates with respect to their nearest jet, and the χ^2 per degree of freedom of the kinematic fit. The $Z\gamma^*$ sample was then defined within the selected $q\bar{q}l^+l^-$ data by mass cuts in the $(M_{\mu^+mu^-}, M_{q\bar{q}})$ and $(M_{e^+e^-}, M_{q\bar{q}})$ planes, requiring the mass of one and only one $f\bar{f}$ pair to be in the Z region; these cuts are defined in figures 4a) and b) for the $q\bar{q}\mu^+\mu^-$ and $q\bar{q}e^+e^-$ samples, respectively. Table 5 summarizes the selection procedures outlined above, showing, for the sum of data over all energy points, the total integrated luminosity, and the numbers of observed and predicted events in the $Z\gamma^*$ region, defined as described above. The selection efficiency (defined as for the ZZ sample described in section 2.2 above) was estimated to be 42% for the $q\bar{q}\mu^+\mu^-$ final state, with a somewhat lower value estimated for the $q\bar{q}e^+e^-$ final state. The backgrounds in the selected samples are small, coming mainly from $q\bar{q}\tau^+\tau^-$, WW and, in the case of $q\bar{q}e^+e^-$, from $q\bar{q}(\gamma)$ production. In the estimation of backgrounds and selection efficiency, the simulation of processes leading to four-fermion final states was done with WPHACT [28], using the JETSET model for quark hadronization, while the $q\bar{q}(\gamma)$ final state was simulated with the KK2f [29] model. Both of these programs were interfaced to the DELPHI simulation program.

Some aspects of the phenomenology of $q\bar{q}l^+l^-$ production in the context of possible neutral triple-gauge-boson couplings, and of the data selected in this final state, are demonstrated in figures 4 and 5. Figures 4a) and b) show the distributions in the $(M_{l^+l^-}, M_{q\bar{q}})$ planes predicted by the Standard Model for the $q\bar{q}\mu^+\mu^-$ and $q\bar{q}e^+e^-$ final

Channel	Integrated luminosity (pb^{-1})	Selected data	Total predicted events	Expected background
$q\bar{q}\mu^+\mu^-$	666.7	35	36.7	3.4
$q\bar{q}e^+e^-$	666.7	39	36.3	6.0

Table 5: $Z\gamma^*$ production: Integrated luminosity, numbers of observed and expected events and predicted background contribution for each topological final state, summed over all energies.

states, respectively. These differ considerably, due to the presence of additional diagrams contributing to $q\bar{q}e^+e^-$ production, in particular those corresponding to the production of Ze^+e^- and $\gamma^*e^+e^-$by t-channel processes. These effects have been discussed fully in [8]. The effect of an anomalous triple-gauge-boson coupling in these channels is illustrated in figures 4c) and d), which show, respectively, the difference between the expected distributions on the ($M_{\mu^+\mu^-}$, $M_{q\bar{q}}$) and ($M_{e^+e^-}$, $M_{q\bar{q}}$) planes when a non-zero contribution from the $d = 8$ operator $\tilde{\mathcal{O}}_4{}^{ZZ\gamma}$ (defined in table 1) is included, and when only the Standard Model amplitudes are used. Again, some differences between the predictions for the $q\bar{q}\mu^+\mu^-$ and $q\bar{q}e^+e^-$ final states are observed; these are due to the presence of additional diagrams in the $q\bar{q}e^+e^-$ amplitude, in this case the V^0V^0 fusion diagram leading to Ze^+e^- production, shown in figure 1d). The overall effect is a negative interference between s- and t-channel amplitudes: for the example shown, the predicted content of figure 4d) ($q\bar{q}e^+e^-$) is $\sim 40\%$ of that of the $q\bar{q}\mu^+\mu^-$ prediction.

Data selected over the whole region of the $q\bar{q}l^+l^-$ phase space are presented in figures 5a) and b) in the form of the distributions of $M_{l^+l^-}$ ($l \equiv \mu, e$) and $M_{q\bar{q}}$. These plots also show the expectations of the Standard Model and of a model in which an anomalous contribution $\tilde{\ell}_4{}^{ZZ\gamma} m_Z^4 = 3.4$ from the operator $\tilde{\mathcal{O}}_4{}^{ZZ\gamma}$ is present.

In the determination of the coupling parameters, the regions in the plane of the masses of the two fermion-antifermion pairs defining the $Z\gamma^*$ samples in the $q\bar{q}\mu^+\mu^-$ and $q\bar{q}e^+e^-$ final states were divided into a small number of bins of unequal size, but containing roughly equal predicted numbers of events; they are shown in figures 4a) and b), respectively. Different bin definitions were made for the two channels, corresponding to those used by DELPHI in [8] in the determination of the $Z\gamma^*$ cross-section. In [8], each of the mass bins defined for the $q\bar{q}e^+e^-$ event sample was further divided into two angular regions, ($40^\circ < \theta_{l^+l^-} < 140^\circ$) and ($\theta_{l^+l^-} < 40^\circ$ or $\theta_{l^+l^-} > 140^\circ$), where $\theta_{l^+l^-}$ is the polar angle of the final state e^+e^- system with respect to the beam direction. These angular regions correspond to DELPHI's barrel and endcap regions, respectively. In the present analysis, we have extended this division to apply to muon as well as electron pairs in the $q\bar{q}l^+l^-$ final states. Binned likelihood fits to the couplings were then made with the bins in ($M_{l^+l^-}, M_{q\bar{q}}$) and $\theta_{l^+l^-}$ thus defined. As in the case of the ZZ final state previously described, the predictions for non-zero neutral gauge boson couplings in the $Z\gamma^*$ data were made by reweighting the simulated samples produced according to the Standard Model with the calculations of DELTGC.

3 Results

In this section the results of our study are presented, expressed in terms of the parameters listed in table 1 describing the neutral triple-gauge-boson effective Lagrangian. In summary, these parameters represent a): the coefficients of the lowest dimension operators contributing to production either of the ZZ and $Z\gamma^*$ final states, or to production of the $Z\gamma$, $Z\gamma^*$ and ZZ final states; in the on-shell ZZ or $Z\gamma$ limit each of these parameters becomes equal to one of the on-shell coefficients f_i^V or h_i^V; b): the coefficients of the lowest dimension operators affecting only the $V^0Z\gamma^*$ vertex; and c): the coefficients of the $SU(2) \times U(1)$-conserving operators describing the $V_1^0V_2^0V_3^0$ vertex in i) the Gounaris-Layssac-Renard and ii) the Alcaraz formulations. (The labels a), b), c) refer to table 1).

Limits on the parameters at the 95% confidence level are given in table 6 and the corresponding likelihood curves are shown in figures 6-10. In all cases, the values quoted are derived from one-parameter fits to the data in the $Z\gamma$, ZZ and $Z\gamma^*$ channels described in sections 2.1, 2.2 and 2.3 above, summing the distributions from different channels where appropriate. In each fit, the values of the other parameters were set to zero, their Standard Model value. For reference, we summarize here the composition of the likelihood function from each of the final states used in the analysis, described in more detail in the sections above: In the $Z\gamma \to \nu\overline{\nu}\gamma$ channel, the number of events with a high energy photon emitted at large polar angle was used in the fit, while in the $Z\gamma\to q\bar{q}\gamma$ channel the fit was performed to the distribution of the decay angle of the Z in its rest frame. In the channels $ZZ \to q\bar{q}l^+l^-$ and $ZZ \to l^+l^-\nu\bar{\nu}$ the distribution of the Z production angle was fitted; in $ZZ \to q\overline{q}q\overline{q}$ and $ZZ \to q\bar{q}\nu\bar{\nu}$ simultaneous fits were made to the Z production angle and, respectively, to the event probability or discriminant variable distributions. In the $Z\gamma^*$ channels studied ($Z\gamma^* \to q\bar{q}\mu^+\mu^-$ and $Z\gamma^* \to q\bar{q}e^+e^-$) the likelihood was evaluated in bins of $q\bar{q}$ or l^+l^- mass and of the polar angle of the detected l^+l^- system. It may be noted that the likelihood distributions examined are derived from a model in which all observables have a quadratic dependence on the fitted parameters, leading to the non-Gaussian distributions seen in many of the plots in figures 6-10.

3.1 Systematic errors

The confidence limits shown in table 6 and the likelihood curves of figures 6-10 include contributions from both statistical and systematic effects. Several sources of systematic error were considered for each of the final states included in the study. These are described below.

In the $\nu\overline{\nu}\gamma$ and $q\bar{q}\gamma$ channels contributing to $Z\gamma$ production, uncertainties of $\pm 1\%$ were assumed in the values assumed for the Standard Model production cross-sections [15, 16], and an experimental uncertainty of $\pm 1\%$ was assumed for the energy calibration of the electromagnetic calorimeter. The effect of an uncertainty of $\pm 1\%$ in the luminosity measurement was also computed, while the uncertainties in the calculations arising from the finite simulated statistics in signal and background channels and from the uncertainty in the knowledge of the background cross-section were found to be negligible in both channels. In the $\nu\overline{\nu}\gamma$ channel, the error due to the uncertainty of $\pm 3\%$ in the trigger efficiency was calculated. In the $q\bar{q}\gamma$ channel, the uncertainty in the use of PYTHIA as the hadronization model was taken into account by comparing events simulated with

Parameter	Channels used	95% Confidence interval	Related on-shell coefficient
a)			
$\tilde{\ell}_1^{ZZZ} m_Z^2$	ZZ $Z\gamma^*$	$[-0.40, +0.42]$	f_4^Z
$\ell_1^{ZZZ} m_Z^2$	ZZ $Z\gamma^*$	$[-0.38, +0.62]$	f_5^Z
$\tilde{\ell}_3^{ZZ\gamma} m_Z^2$	ZZ $Z\gamma^*$	$[-0.23, +0.25]$	f_4^γ
$\ell_2^{ZZ\gamma} m_Z^2$	ZZ $Z\gamma^*$	$[-0.52, +0.48]$	f_5^γ
$\tilde{\ell}_1^{ZZ\gamma} m_Z^2$	$Z\gamma$ $Z\gamma^*$ ZZ	$[-0.23, +0.23]$	h_1^Z
$\ell_1^{ZZ\gamma} m_Z^2$	$Z\gamma$ $Z\gamma^*$ ZZ	$[-0.30, +0.16]$	h_3^Z
$\tilde{\ell}_1^{Z\gamma\gamma} m_Z^2$	$Z\gamma$ $Z\gamma^*$ ZZ	$[-0.14, +0.14]$	h_1^γ
$\ell_1^{Z\gamma\gamma} m_Z^2$	$Z\gamma$ $Z\gamma^*$ ZZ	$[-0.049, +0.044]$	h_3^γ
b)			
$\tilde{\ell}_4^{ZZ\gamma} m_Z^4$	ZZ $Z\gamma^*$	$[-1.67, +1.92]$	–
$\ell_2^{Z\gamma\gamma} m_Z^4$	ZZ $Z\gamma^*$	$[-0.49, +0.61]$	–
c) i)			
$-\cot\theta_W m_Z^2 \frac{v^2}{4} \tilde{\ell}_{SU(2)\times U(1)}$	$Z\gamma$ $Z\gamma^*$ ZZ	$[-0.13, +0.13]$	h_1^γ
$-\cot\theta_W m_Z^2 \frac{v^2}{4} \ell_{SU(2)\times U(1)}$	$Z\gamma$ $Z\gamma^*$ ZZ	$[-0.045, +0.047]$	h_3^γ
ii)			
$-\cot\theta_W m_Z^2 \frac{v^2}{4} \tilde{\ell}_8^A$	$Z\gamma$ $Z\gamma^*$ ZZ	$[-0.14, +0.14]$	h_1^γ
$-\cot\theta_W m_Z^2 \frac{v^2}{4} \ell_8^A$	$Z\gamma$ $Z\gamma^*$ ZZ	$[-0.049, +0.045]$	h_3^γ
$-\cot\theta_W m_Z^2 \frac{v^2}{4} \tilde{\ell}_8^B$	$Z\gamma$ $Z\gamma^*$ ZZ	$[-0.23, +0.24]$	h_1^Z
$-\cot\theta_W m_Z^2 \frac{v^2}{4} \ell_8^B$	$Z\gamma$ $Z\gamma^*$ ZZ	$[-0.30, +0.18]$	h_3^Z

Table 6: Results of the study of neutral gauge couplings. For each of the parameters listed in table 1, the table shows the experimental channels used and the 95% confidence limits obtained. The right-most column indicates the parameter which, in the on-shell limit, is equal to the parameter determined. In the determination of any one coupling, the values of all the others were held at their Standard Model values. The limits shown include both statistical and systematic effects: a) Coefficients of lowest dimension operators contributing either to ZZ and $Z\gamma^*$ production or to $Z\gamma$, $Z\gamma^*$ and ZZ production; b) Coefficients of lowest dimension operators affecting only the $V^0 Z\gamma^*$ vertices; c) Coefficients of $SU(2)\times U(1)$-conserving operators according to i) the Gounaris-Layssac-Renard constraints and ii) the Alcaraz constraints (see text, section 1.1).

PYTHIA and HERWIG [30]; this gave rise to an estimated systematic error of +1.7% from this source. In the combination of data at different energies, all the above effects were considered as correlated. The resulting overall systematic error in the coupling parameters was found to be of the order of 30% of the statistical errors in the case of h_1^Z and h_3^Z, about 50% of the statistical error for h_1^γ, and of the same order as the statistical error for h_3^γ.

A full description of the treatment of systematic effects in the channels contributing to ZZ production has been given in [7]. In the $q\bar{q}q\bar{q}$ channel, the dominant effect arises from uncertainties in the modelling of the main source of background, namely production of the $q\bar{q}(\gamma)$ final state, when the subsequent hadronization of the quarks gives rise to several jets. In the present study, the effect of this background was estimated by assuming an uncertainty of $\pm 5\%$ in the $q\bar{q}(\gamma)$ production cross-section. In the $q\bar{q}l^+l^-$ channel, the dominant systematic effect relevant to the present study comes from the uncertainty in the efficiency for selecting $q\bar{q}e^+e^-$ and $q\bar{q}\mu^+\mu^-$ events, taken to be $\pm 3\%$. In addition, in the $q\bar{q}e^+e^-$ channel a systematic error of $\pm 1.6\%$ was estimated to arise from the uncertainty in the calculation of the background level. In the $q\bar{q}\nu\bar{\nu}$ channel, as in $q\bar{q}q\bar{q}$, the main source of systematic error arises from modelling of the $q\bar{q}(\gamma)$ background, in this case corresponding to the kinematic region with large missing energy, and hence low visible $q\bar{q}$ energy. A study of the energy flow in this region using events at the Z peak allowed a determination of the effect of this uncertainty in the present analysis; it gives rise to systematic errors in the coupling parameters of order 5% - 10% of the values of the statistical errors. Another, comparable source of systematic error in this channel comes from the uncertainties in the cross-sections for the dominant background channels, particularly $We\nu$ production. Systematic effects in the $l^+l^-\nu\bar{\nu}$ channels were found to be negligible. In addition, the effects of uncertainties of $\pm 2\%$ in the overall ZZ cross-section and of $\pm 1\%$ in the luminosity measurement were considered. The combined effect of all the systematic uncertainties in the channels contributing to ZZ production is small, typically $\sim 15\%$ of the statistical errors.

The systematic uncertainties in the study of the $q\bar{q}e^+e^-$ and $q\bar{q}\mu^+\mu^-$ channels contributing to $Z\gamma^*$ production have been described in [8]. Several effects, including uncertainties in lepton identification, the effect of limited simulated data and, in the $q\bar{q}e^+e^-$ channel, identification of fake electrons coming from background channels, combine to give a systematic error on the efficiency to select $q\bar{q}e^+e^-$ and $q\bar{q}\mu^+\mu^-$ events of $\pm 5\%$ and a relative uncertainty in the background level of $\pm 15\%$. In addition, a systematic error of $\pm 1\%$ in the luminosity measurement was assumed. The overall effect of these systematic uncertainties in the determination of the coupling parameters is small in comparison with the statistical errors; in the case of the parameters listed in table 6b) they amount to $\sim$15% and $\sim$5% of the statistical errors for ${\ell_2}^{Z\gamma\gamma}$ and ${\tilde{\ell}_4}^{ZZ\gamma}$, respectively.

In the combination of data from the different final states, $Z\gamma$, ZZ and $Z\gamma^*$, all the systematic effects listed above were treated as uncorrelated except those arising from the uncertainty in the luminosity measurement.

3.2 Discussion

A few comments may be made on the results shown in table 6 and figures 6-10.

All the results are compatible with the Standard Model expectation of the absence of neutral trilinear gauge boson couplings. The results shown in table 6a) and figures 6

and 7 demonstrate this conclusion in the effective Lagrangian model of reference [2] for the $d = 6$ operators contributing to on-shell $Z\gamma$, off-shell $Z\gamma^*$ and on-shell ZZ production, or to on-shell ZZ and off-shell $Z\gamma^*$ production. As mentioned in section 1.1 (and predicted from simulated studies [5]), the contribution of the data from the channels populated only by off-shell production processes to the limits determined on these parameters is small: determination of these parameters using only such data leads to precisions poorer by factors of $\sim 3 - 7$ than those using on-shell $Z\gamma$ or ZZ data. (This effect is observed most strongly in the case of the determination of h_3^γ, where the interference in the squared matrix element between the anomalous and Standard Model amplitudes leads to a relatively precise determination of this parameter). Thus these results, with negligible changes, may also be interpreted in terms of the parameters h_i^V and f_i^V of on-shell $Z\gamma$ and ZZ production, listed in the right-hand column of the table, and they may be compared directly with other published results for these on-shell parameters.

The results shown in table 6b) and figure 8 examine the possibility of four-fermion production via an anomalous $V^0 Z\gamma^*$ vertex by determining the coefficients of the lowest dimension ($d = 8$) operators in the model of reference [2] which would contribute to such a process. As noted in section 1.1, contributions from these operators affect both the $Z\gamma^*$ and ZZ final states, the experimental samples from the two final states contributing roughly equally to the log likelihood distribution in the combination of the data. The results of the fits show that there is no evidence in the data for a CP-conserving anomalous coupling at the $\gamma Z\gamma^*$ vertex or for a CP-violating coupling at the $ZZ\gamma^*$ vertex.

The results shown in table 6c) and figures 9 and 10 indicate that there is no evidence in the data for $SU(2) \times U(1)$-conserving anomalous couplings in the models of references [2] and [5]. Here again, in the combinations of data from different final states, the contributions from $Z\gamma$ production dominate, as can be seen by comparison of the likelihood curves of figure 7 and either figure 9 or figure 10, and from the confidence limits shown in the table. This arises both because of the sensitivity to h_3^γ noted above and because of the greater statistical contribution from $Z\gamma$ compared to that from ZZ production at LEP2 energies.

Finally, we note from previous analyses of the $Z\gamma$ and ZZ final states [31], similar to those presented here, that strong correlations are observed between the parameters h_3^γ and h_3^Z determined from analysis of the $Z\gamma$ final state, while the parameter pairs $(h_1^\gamma,\, h_1^Z)$, $(f_4^\gamma,\, f_4^Z)$ and $(f_5^\gamma,\, f_5^Z)$ show little correlation.

4 Conclusions

A study has been performed of the neutral triple-gauge-boson vertex using DELPHI data from the final states $Z\gamma$, ZZ and $Z\gamma^*$ produced at LEP2. The results have been interpreted in terms of various models of the interaction Lagrangian proposed in the literature. We find no evidence for the production of these states by processes involving neutral triple-gauge-boson vertices with either one or two off-shell bosons, nor when the data are analyzed in terms of models in which the neutral triple-gauge-boson vertex is constrained to be $SU(2) \times U(1)$-conserving. These conclusions are in agreement with the predictions of the Standard Model.

Acknowledgements

We are greatly indebted to our technical collaborators, to former members of the CERN-SL division for their excellent performance of the LEP collider, and to the funding agencies for their support in building and operating the DELPHI detector.
We acknowledge in particular the support of
Austrian Federal Ministry of Science and Traffics, GZ 616.364/2-III/2a/98,
FNRS–FWO, Belgium,
FINEP, CNPq, CAPES, FUJB and FAPERJ, Brazil,
Czech Ministry of Industry and Trade, GA CR 202/96/0450 and GA AVCR A1010521,
Danish Natural Research Council,
Commission of the European Communities (DG XII),
Direction des Sciences de la Matière, CEA, France,
Bundesministerium für Bildung, Wissenschaft, Forschung und Technologie, Germany,
General Secretariat for Research and Technology, Greece,
National Science Foundation (NWO) and Foundation for Research on Matter (FOM), The Netherlands,
Norwegian Research Council,
State Committee for Scientific Research, Poland, 2P03B06015, 2P03B1116 and SPUB/P03/178/98,
JNICT–Junta Nacional de Investigação Científica e Tecnológica, Portugal,
Vedecka grantova agentura MS SR, Slovakia, Nr. 95/5195/134,
Ministry of Science and Technology of the Republic of Slovenia,
CICYT, Spain, AEN96–1661 and AEN96-1681,
The Swedish Natural Science Research Council,
Particle Physics and Astronomy Research Council, UK,
Department of Energy, USA, DE–FG02–94ER40817.

References

[1] K. Hagiwara *et al.*, Nucl. Phys. **B282** (1987) 253.

[2] G.J. Gounaris, J. Layssac and F.M. Renard, Phys. Rev. **D62** (2000) 073012.

[3] M.S. Bilenky *et al.*, Nucl. Phys. **B409** (1993) 22.

[4] G. Gounaris *et al.*, in *Physics at LEP2*, eds. G. Altarelli, T. Sjöstrand and F. Zwirner, CERN 96-01 (1996) Vol.1, 525.

[5] J. Alcaraz, Phys.Rev. **D65** (2002) 075020.

[6] DELPHI Collaboration, W. Adam *et al.*, Phys. Lett. **B380** (1996) 471;
DELPHI Collaboration, P. Abreu *et al.*, Phys. Lett. **B423** (1998) 194.

[7] DELPHI Collaboration, J. Abdallah *et al.*, Eur. Phys. J. **C30** (2003) 447.

[8] DELPHI Collaboration, J. Abdallah *et al.*, *$Z\gamma^*$ production in e^+e^- interactions at $\sqrt{s}$ = 183 - 209 GeV*, in preparation, to be submitted to Eur. Phys. J.

[9] ALEPH Collaboration, ALEPH 2001-061 CONF 2001-041 (2001);
L3 Collaboration, P. Achard *et al.*, Phys. Lett. **B572** (2003) 133;
L3 Collaboration, P. Achard *et al.*, Phys. Lett. **B597** (2004) 145;
OPAL Collaboration G. Abbiendi *et al.*, Eur. Phys. J. **C17** (2000) 553;
OPAL Collaboration, G. Abbiendi *et al.*, Eur. Phys. J. **C32** (2004) 303.

[10] DELPHI Collaboration, P. Aarnio *et al.*, Nucl. Instr. and Meth. **A303** (1991) 233.

[11] DELPHI Trigger Group, A. Augustinus *et al.*, Nucl. Instr. and Meth. **A515** (2003) 782.

[12] DELPHI Collaboration, P. Abreu *et al.*, Nucl. Instr. and Meth. **A378** (1996) 57.

[13] DELPHI Silicon Tracker Group, P. Chochula *et al.*, Nucl. Instr. and Meth. **A412** (1998) 304.

[14] DELPHI Collaboration, J. Abdallah *et al.*, Eur. Phys. J. **C38** (2005) 395.

[15] G. Montagna *et al.*, Nucl. Phys. **B452** (1995) 161.

[16] S. Jadach, B.F.L. Ward and Z. Was, Comp. Phys. Comm. **79** (1994) 503.

[17] P. Abreu *et al.*, Nucl. Instr. and Meth. **A427** (1999) 487.

[18] T.Sjöstrand, *PYTHIA 5.7 / JETSET 7.4*, CERN-TH 7112/93 (1993).

[19] U. Baur and E.L. Berger, Phys. Rev. **D47** (1993) 4889.

[20] G.J. Gounaris, J. Layssac and F.M. Renard, Phys. Rev. **D61** (2000) 073013.

[21] T.G.M. Malmgren, Comp. Phys. Comm. **106** (1997) 230;
T.G.M. Malmgren and K.E. Johansson, Nucl. Inst. and Meth. **403** (1998) 481.

[22] F.A. Berends, R. Pittau and R. Kleiss, Comp. Phys. Comm. **85** (1995) 437.

[23] J. Fujimoto *et al.*, Comp. Phys. Comm. **100** (1997) 128.

[24] S. Jadach, W. Placzek and B.F.L. Ward, Phys. Lett. **B390** (1997) 298.

[25] T. Alderweireld *et al.*, in *Reports of the Working Groups on Precision Calculations for LEP2 Physics*, eds. S. Jadach, G. Passarino and R. Pittau, CERN 2000-009 (2000) 219.

[26] F.A. Berends, P.H. Daverveldt and R. Kleiss, Comp. Phys. Comm. **40** (1986) 271, 285 and 309.

[27] O.P. Yushchenko and V.V. Kostyukhin, *DELTGC - A program for four-fermion calculations*, DELPHI 99-4 PHYS 816 (1999).

[28] E. Accomando and A. Ballestrero, Comp. Phys. Comm. **99** (1997) 270;
E. Accomando, A. Ballestrero and E. Maina, Comp. Phys. Comm. **150** (2003) 166;
A. Ballestrero, R. Chierici, F. Cossutti and E. Migliore, Comp. Phys. Comm. **152** (2003) 175.

[29] S. Jadach, B.F.L. Ward and Z. Was, Comp. Phys. Comm. **130** (2000) 260.

[30] G. Marchesini *et al.*, Comp. Phys. Comm. **67** (1992) 465.

[31] P. Bambade *et al.*, DELPHI 2001-097 CONF 525 (2001).

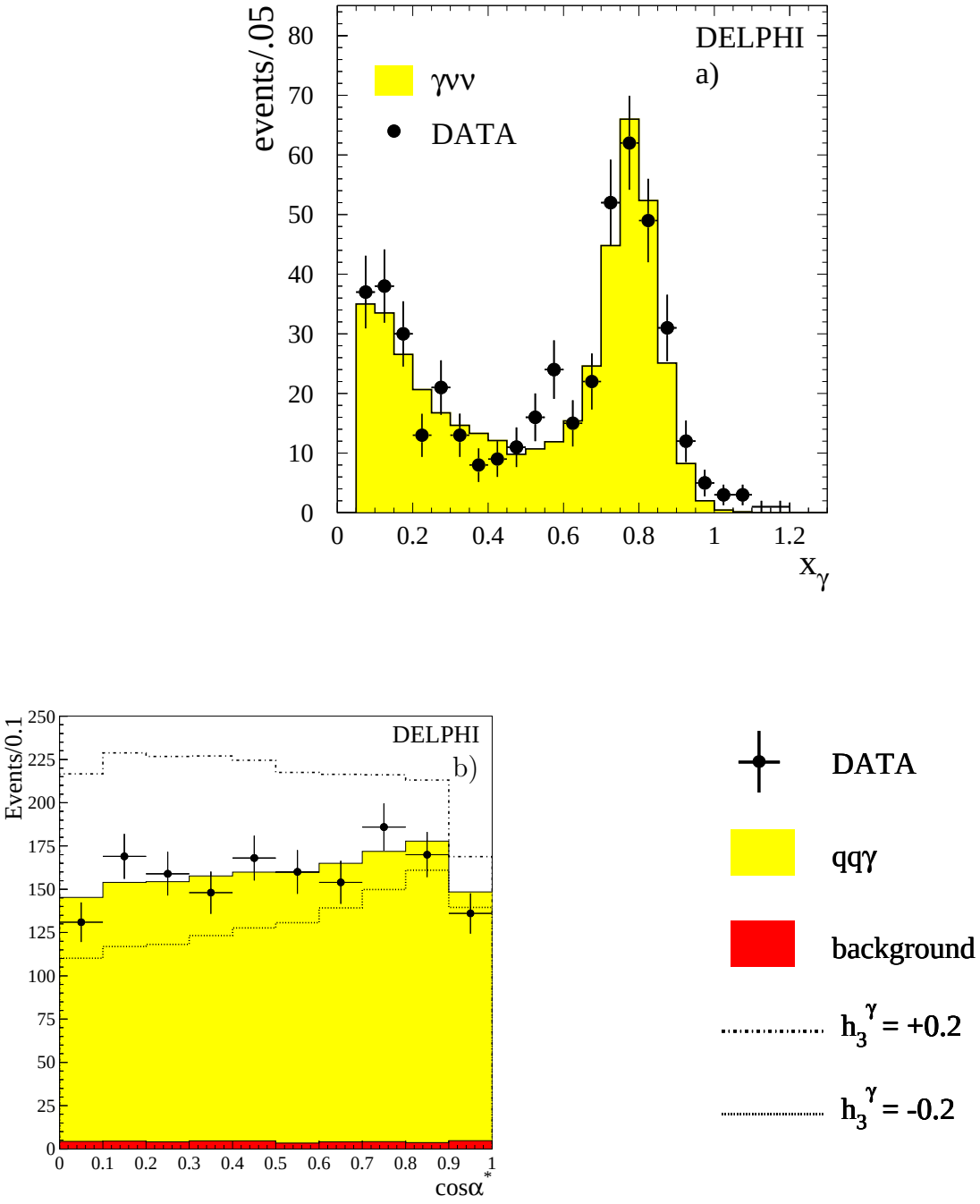

Figure 2: a) Distribution of $x_\gamma = E_\gamma/E_{beam}$, the energy of identified photons normalized to the beam energy in the data in the $\nu\overline{\nu}\gamma$ channel, summed over all energy points. The distribution is shown before imposing the experimental cut at $E_\gamma = 50$ GeV. The experimental data points are shown by dots and the shaded histogram shows the predictions of the Standard Model for signal plus background. (The background contribution is very small, and is not shown separately). b) Distribution of the decay angle, $\cos\alpha^\star$, of the quark (or antiquark) in the Z centre-of-mass frame for data selected in the $q\bar{q}\gamma$ channel. The experimental data points are shown by dots, the shaded histogram shows the predictions of the Standard Model for signal and background, and the outlined histograms the expectations for values of $h_3^\gamma = \pm 0.2$.

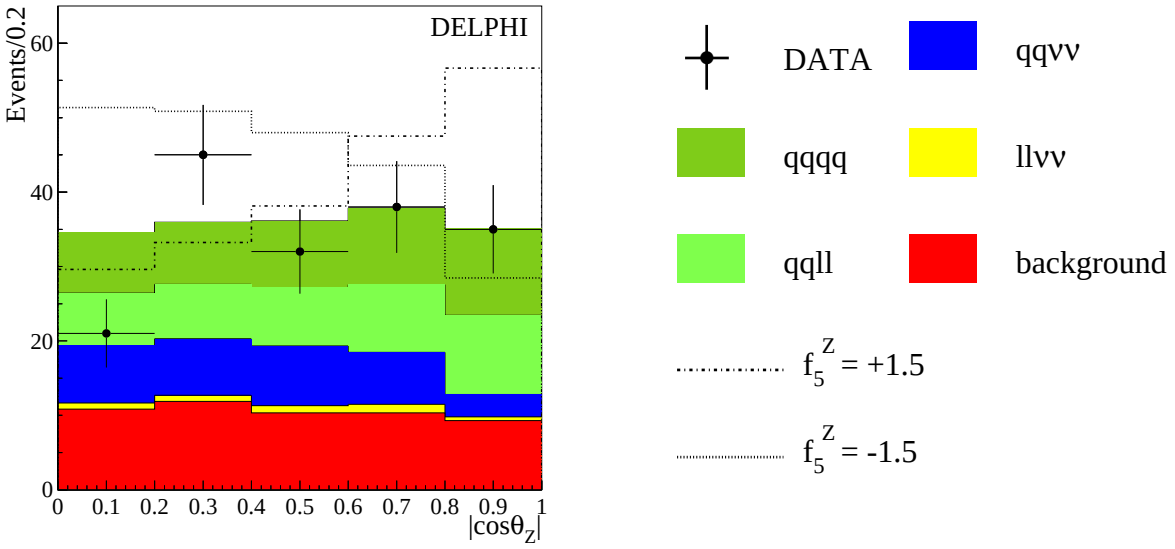

Figure 3: Distribution of $|\cos\theta_Z|$ where θ_Z is the polar angle of the ZZ system, for data selected in the ZZ channels. The experimental data points are shown by dots, the shaded histogram shows the predictions of the Standard Model for signal and background, and the outlined histograms the expectations for values of $f_5^Z = \pm 1.5$.

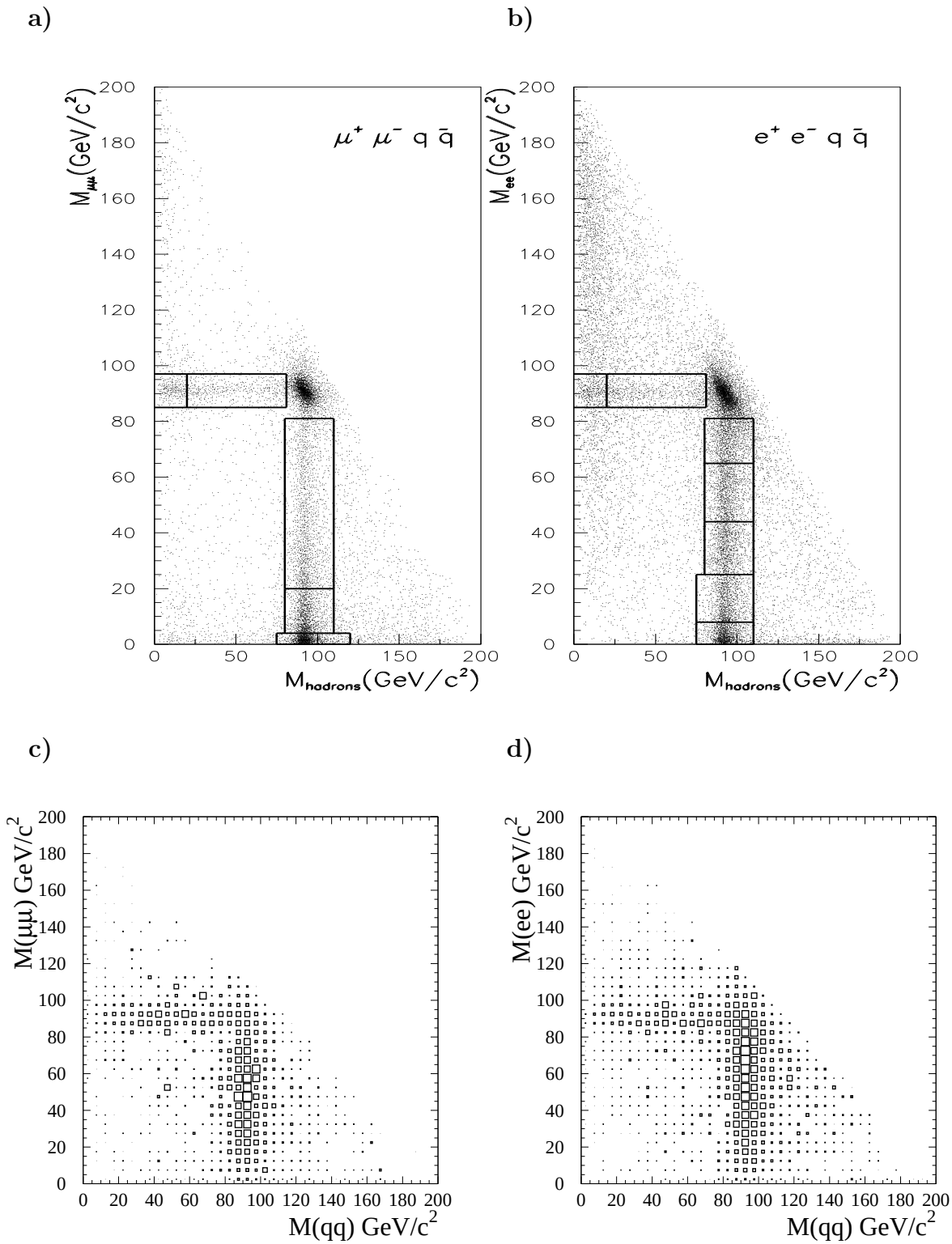

Figure 4: For the $q\bar{q}l^+l^-$ final state: predicted Standard Model distributions of events a) in the ($M_{q\bar{q}}$, $M_{\mu^+\mu^-}$) plane, and b) in the ($M_{q\bar{q}}$, $M_{e^+e^-}$) plane, showing the bins used in the fits to the coupling parameters. The sum of all the bins defines the $Z\gamma^*$ sample. c) Expected distribution in the ($M_{q\bar{q}}$, $M_{\mu^+\mu^-}$) plane, and d) in the ($M_{q\bar{q}}$, $M_{e^+e^-}$) plane, of the difference between the predictions of the Standard Model plus an anomalous contribution, $\tilde{\ell}_4^{ZZ\gamma} m_Z^4 = 3.4$, and the Standard Model only. (The parameter $\tilde{\ell}_4^{ZZ\gamma}$ is defined in table 1). Plots a) and b) and, separately, c) and d) were computed with the same assumed luminosities.

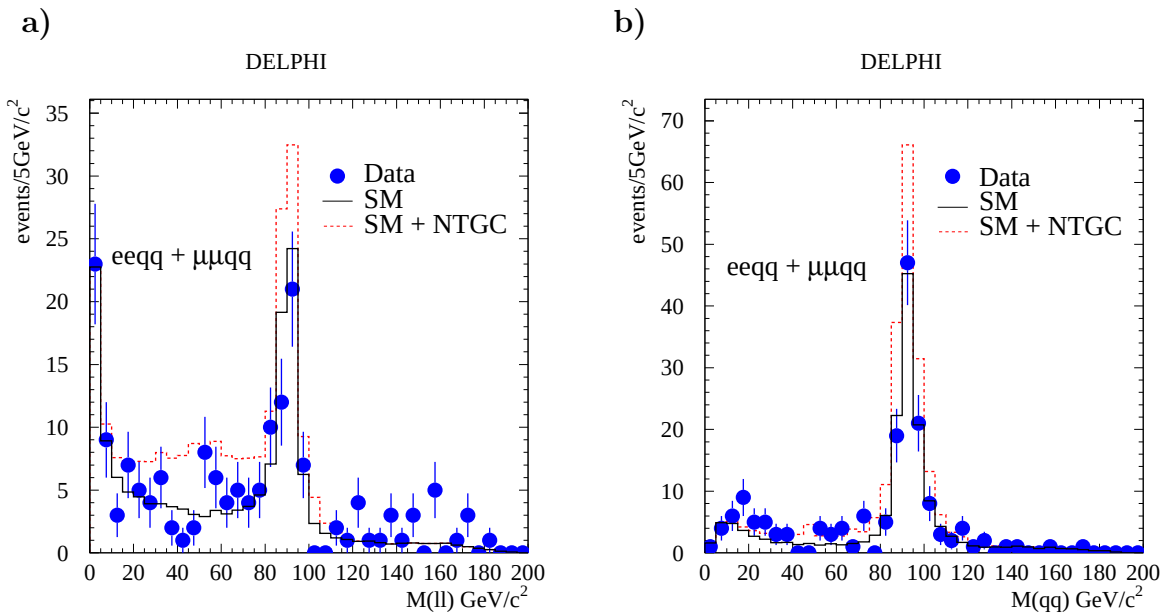

Figure 5: a) Distribution of $M_{l^+l^-}$ ($l \equiv e, \mu$), and b) of $M_{q\bar{q}}$, for data selected in the $q\bar{q}\mu^+\mu^-$ and $q\bar{q}e^+e^-$ channels. The experimental data points are shown by dots, the full histograms show the predictions of the Standard Model for signal and background, and the dotted histograms the expectations when an anomalous contribution, $\tilde{\ell}_4^{ZZ\gamma} m_Z^4 = 3.4$, is present.

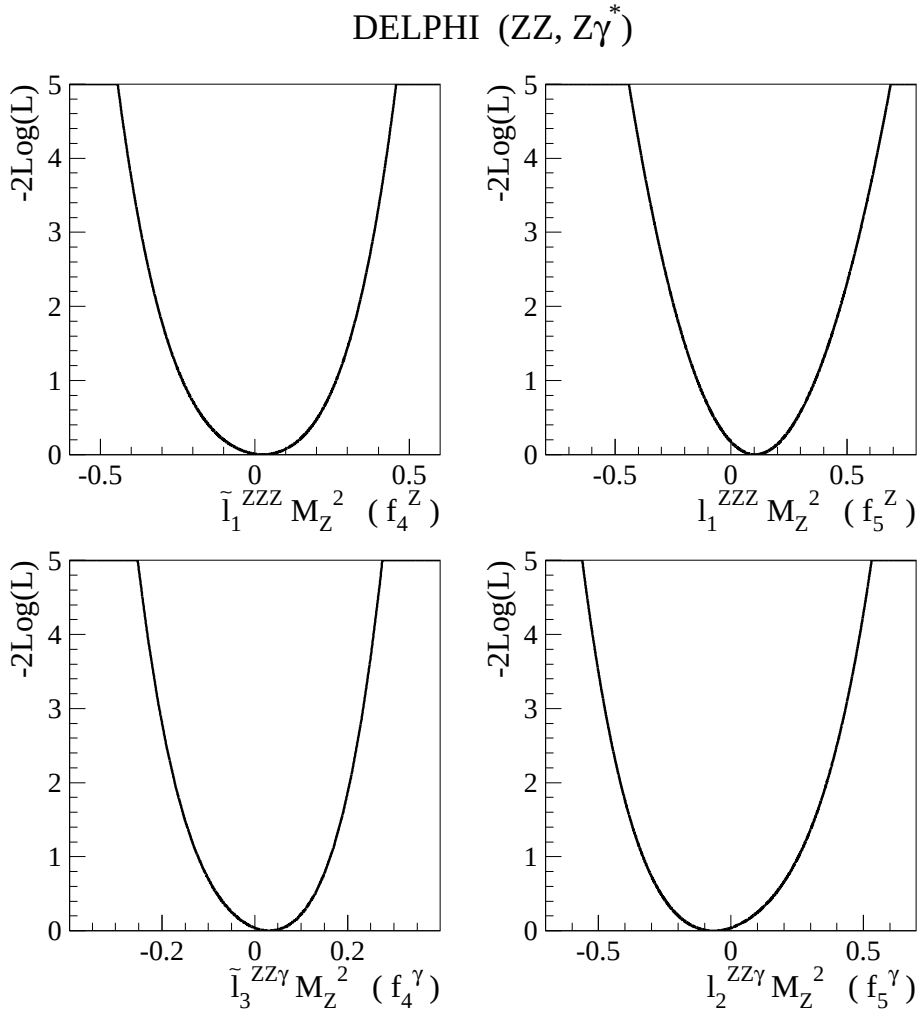

Figure 6: Likelihood distributions for neutral gauge coupling parameters corresponding to Lagrangian operators influencing ZZ and $Z\gamma^*$ production. The parameters are defined in section 1.1; the corresponding on-shell parameters are shown in parentheses on the abscissa labels. The distributions include the contributions from both statistical and systematic effects.

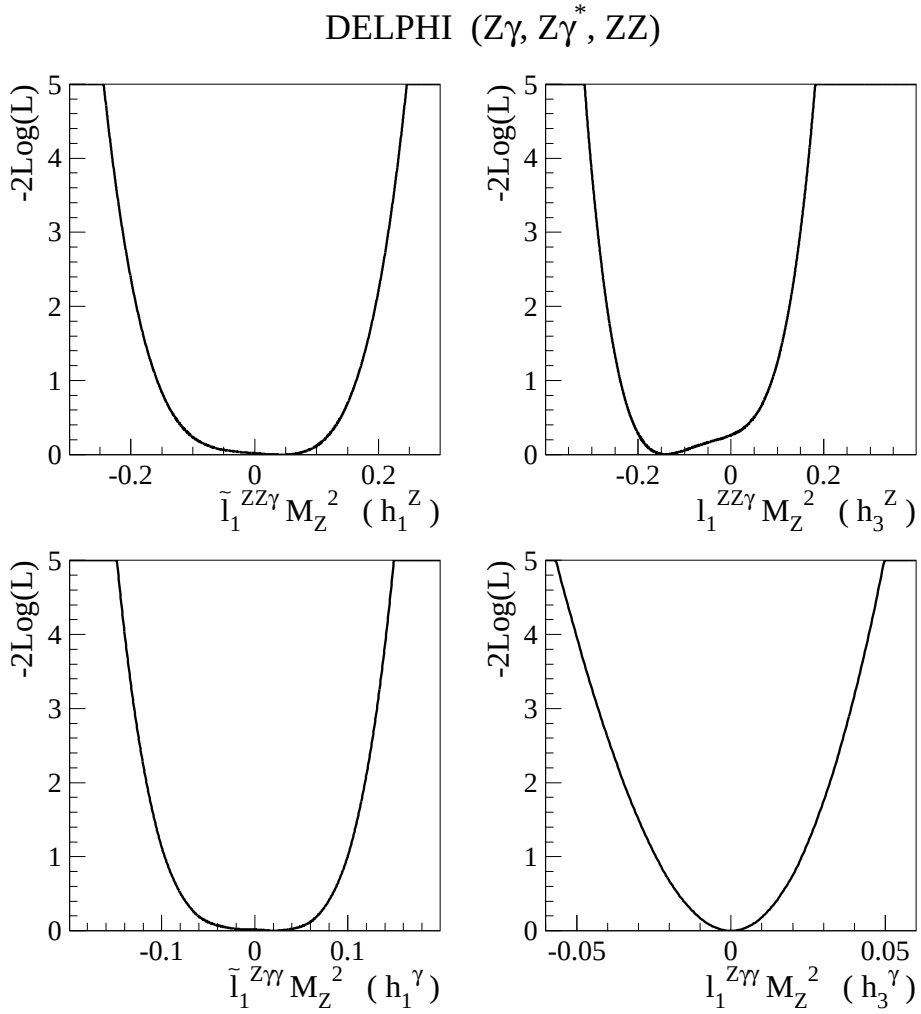

Figure 7: Likelihood distributions for neutral gauge coupling parameters corresponding to Lagrangian operators influencing $Z\gamma$, $Z\gamma^*$ and ZZ production. The parameters are defined in section 1.1; the corresponding on-shell parameters are shown in parentheses on the abscissa labels. The distributions include the contributions from both statistical and systematic effects.

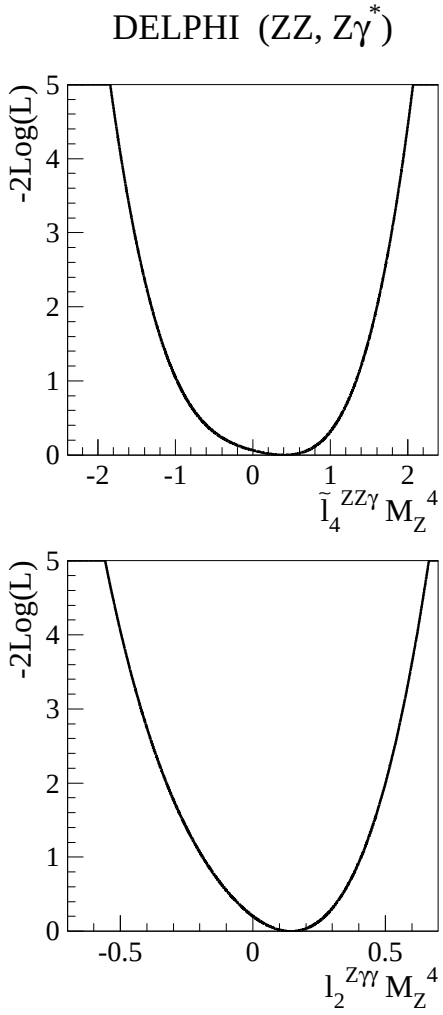

Figure 8: Likelihood distributions for neutral gauge coupling parameters corresponding to Lagrangian operators affecting only the $V^0 Z\gamma^*$ vertices. The parameters are defined in section 1.1. The distributions include the contributions from both statistical and systematic effects.

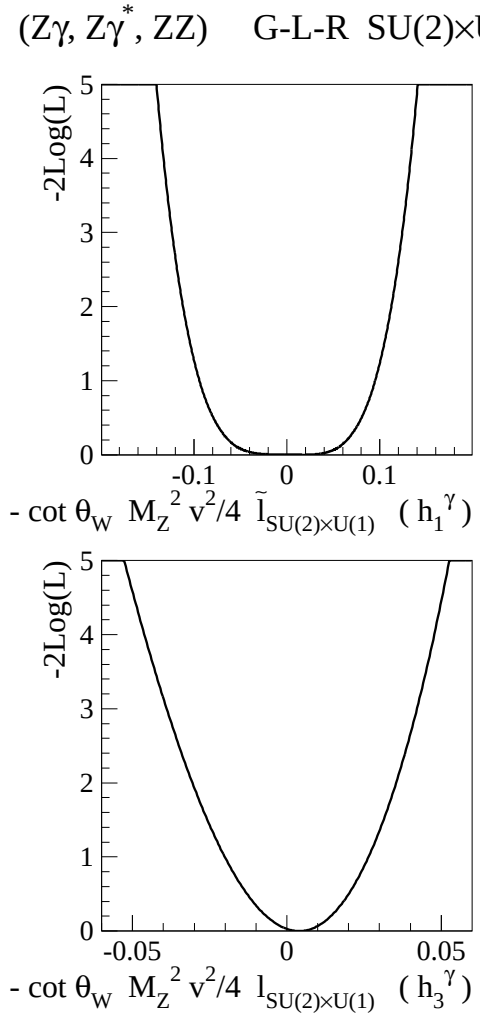

Figure 9: Likelihood distributions for neutral gauge coupling parameters corresponding to $SU(2) \times U(1)$-conserving Lagrangian operators satisfying the Gounaris-Layssac-Renard (G-L-R) constraints. The parameters are defined in section 1.1. The distributions include the contributions from both statistical and systematic effects.

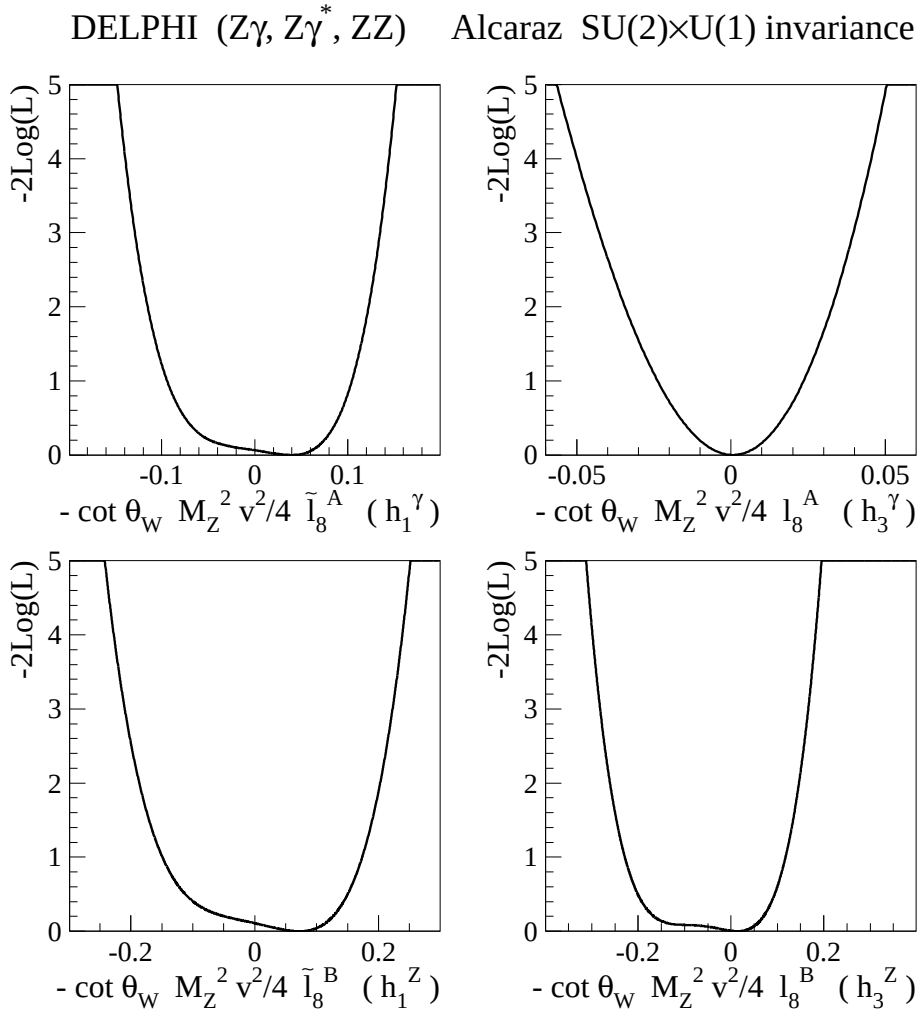

Figure 10: Likelihood distributions for neutral gauge coupling parameters corresponding to $SU(2) \times U(1)$-conserving Lagrangian operators satisfying the Alcaraz constraints. The parameters are defined in section 1.1.